

# 金字塔型点阵夹芯梁振动特性分析\*

施月奇 陈建恩<sup>†</sup> 葛为民 刘军 王肖锋

(天津理工大学 天津市先进机电系统设计 with 智能控制重点实验室, 天津 300384)

**摘要** 研究了金字塔芯层点阵夹芯梁的自由振动和非线性受迫振动特性. 基于折线理论推导出两端简支金字塔型点阵夹芯梁的非线性动力学方程. 计算点阵夹芯梁固有频率并进行了验证. 分析了杆件半径、杆件倾斜角度和芯层高度对点阵夹芯梁固有频率的影响. 研究了点阵夹芯梁在不同激励幅值和不同结构参数下的非线性幅频响应特性. 结果表明, 随着各结构参数的增大, 夹芯梁的固有频率均呈先增大后减小的变化规律, 并且芯层结构参数对点阵夹芯梁的非线性响应存在复杂影响.

**关键词** 振动分析, 点阵夹芯梁, 非线性幅频响应, 结构参数, 固有频率

DOI: 10.6052/1672-6553-2017-055

## 引言

点阵材料是一种模拟分子点阵构型制造出的周期性超轻多孔材料, 具有高比强度、高比刚度、耐冲击等特点, 并且具有高效散热、隔热, 吸声效果佳, 吸收电磁波等功能. 点阵材料具有良好的可设计性, 根据不同应用需求, 可以对其细观结构进行多功能、多学科协同设计. 点阵材料的研究, 在航空航天、交通、海洋采油等高科技领域中有着重要的意义. 值得指出的是, 多孔材料和结构在高能耗装备(高速列车、航空航天器、轮船等)的广泛应用, 不仅会大幅度降低对常规能源的需求, 同时也可减少环境污染<sup>[1-3]</sup>. 点阵材料被国际上公认为最具发展前景的轻质多孔材料<sup>[4]</sup>, 其应用和发展可以在较大程度上对蜂窝、泡沫等传统多孔材料进行替代和补充.

点阵夹芯结构在航空航天领域应用广泛, 如飞机机翼、航空器舱板、卫星主体结构等. 飞行器在高速飞行中会在气动载荷的作用下进行受迫振动, 卫星在轨道和姿态调节时亦会发生自由振动, 这些振动对飞行器存在不同程度的危害. 因此, 研究点阵夹芯结构的振动特性以便于对其进行振动控制, 进而降低事故的发生率, 保障飞行器的安全运行, 对于航空航天事业具有重要的意义. Song 和 Li<sup>[5]</sup> 利用

Reddy 三阶剪切变形理论研究了金字塔型点阵夹芯梁的气动弹性问题. 娄佳等<sup>[6]</sup> 研究了复合材料四面体点阵夹芯梁的自由振动特性. Chen<sup>[7]</sup> 等研究了点阵夹芯板的非线性振动特性. 李拓、江俊<sup>[8]</sup> 应用分解刚度法获得四边简支点阵夹芯板的固有频率, 以芯层高度和桁架杆截面尺寸为设计变量, 以第一阶频率最大化为目标对夹芯板进行了优化. 在传统夹芯结构的研究方面, Kant 和 Swaminathan<sup>[9]</sup> 基于高阶精化理论, 研究了简支边界条件下复合材料层合夹芯板的固有频率. Alijani 和 Amabili<sup>[10,11]</sup> 运用基于 Lagrange 方程的多模态能量法, 研究了自由边界条件下矩形夹芯板的非线性振动特性. Won 等<sup>[12]</sup> 推导出具有三层对称阻尼的夹层梁的动力学方程, 研究了粘弹性夹芯梁非线性振动响应. 当前, 对于传统夹芯结构的振动特性已有深入研究, 然而对于点阵夹芯结构动力学特性的理论研究十分有限, 对于点阵夹芯结构非线性振动特性的研究更加缺乏.

本文对两端简支金字塔型点阵夹芯梁的振动特性进行深入分析. 将芯层等效为连续均匀材料, 采用折线理论描述夹芯梁蒙皮和芯层的几何变形. 推导出金字塔型点阵夹芯梁的非线性振动方程. 分析杆件半径、杆件倾斜角度以及芯层高度对点阵夹芯梁固有频率的影响, 研究点阵夹芯梁在不同激励幅值和不同结构参数下的非线性幅频响应特性.

2016-07-20 收到第 1 稿, 2016-09-09 收到修改稿.

\* 国家自然科学基金(11402170)、天津市自然科学基金(14JCYBJC19400)

<sup>†</sup> 通讯作者 E-mail: vchenje@163.com

# 1 理论计算

## 1.1 等效参数

图1为一段点阵夹芯梁的示意图,  $x$ 轴与梁的中线重合,  $z$ 轴垂直于梁的中线,  $d$ 表示上下蒙皮中面的距离,  $h$ 表示梁的总厚度,  $h_c$ 表示芯层的厚度,  $h_f$ 表示蒙皮的厚度. 本文基于 Allen<sup>[13]</sup>的经典夹芯梁理论做如下假设:

- (1) 点阵夹芯梁在变形过程中厚度不变, 即挠度  $w$  与  $z$  值无关;
- (2) 只考虑蒙皮的弯曲变形, 忽略蒙皮的剪切变形;
- (3) 只考虑芯层的剪切变形, 忽略其弯曲变形.

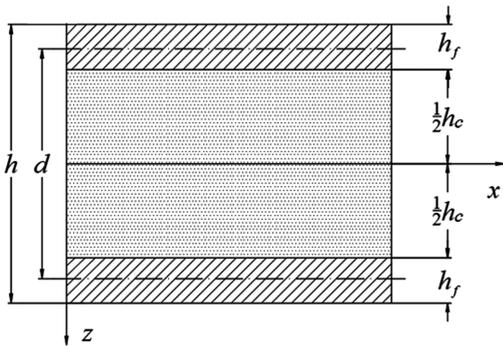


图1 点阵夹芯梁片段示意图

Fig. 1 Sketch of a part of a truss core sandwich beam

该假设被广泛应用于夹芯结构的研究. 图2为金字塔型点阵夹芯梁芯层的一个单胞. 其中,  $r_c$ 表示杆件半径,  $\alpha$ 表示杆件的倾角,  $l$ 表示杆件长度.  $\rho_c$ 、 $\rho$ 和 $\bar{\rho}$ 分别表示芯层母体材料密度、芯层等效密度和芯层相对密度, 则有:

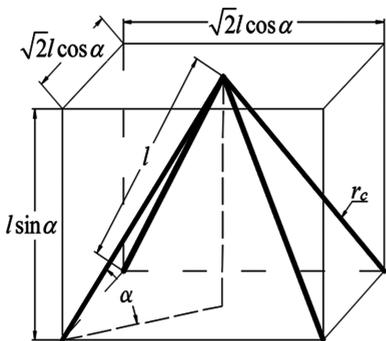


图2 金字塔点阵芯层的晶胞单元

Fig. 2 A unit cell of pyramidal truss core

$$\bar{\rho} = \frac{\rho_c}{\rho} = \frac{2\pi r_c^2}{l^2 \cos^2 \alpha \sin \alpha} \quad (1)$$

$E$ 表示芯层母体材料的弹性模量, 芯层的等效

剪切模量  $G_c$  由参考文献[14]给出:

$$G_c = \frac{1}{8} E \sin^2(2\alpha) \bar{\rho} \quad (2)$$

## 1.2 动力学方程

点阵夹芯梁在变形前后的几何形状如图3所示. 基于 Allen 假设, 夹芯梁的上下蒙皮只发生弯曲变形, 芯层只发生剪切变形. 运用折线理论<sup>[15]</sup>描述蒙皮和芯层变形, 得到夹芯梁任意点沿  $x$  和  $z$  轴方向的位移如下:

$$-\frac{h}{2} \leq z \leq -\frac{h_c}{2}, w_t = w_0, \quad (3a)$$

$$u_t = u_0 - z \frac{\partial w_0}{\partial x} + \frac{h_c}{2} \left( \varphi_x - \frac{\partial w_0}{\partial x} \right) \quad (3a)$$

$$-\frac{h_c}{2} \leq z \leq \frac{h_c}{2}, u_c = u_0 - z \varphi_x, w_c = w_0 \quad (3b)$$

$$\frac{h_c}{2} \leq z \leq \frac{h}{2}, w_b = w_0, \quad (3c)$$

$$u_b = u_0 - z \frac{\partial w_0}{\partial x} - \frac{h_c}{2} \left( \varphi_x - \frac{\partial w_0}{\partial x} \right) \quad (3c)$$

式中,  $u$ 、 $w$  分别表示梁在  $x$  轴和  $z$  轴方向的位移,  $\varphi_x$  表示芯层截面的转角, 下标  $0$ 、 $t$ 、 $b$ 、 $c$  分别表示中性面、上面板、下面板和芯层.

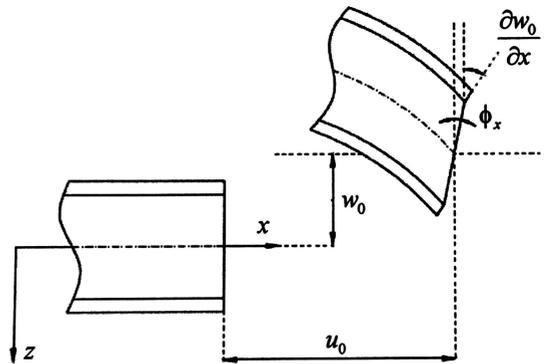


图3 变形前后的夹芯梁几何形状

Fig. 3 Undeformed and deformed geometries of a sandwich beam

根据冯卡门大变形理论, 点阵夹芯梁的非线性应变位移关系可表述为:

$$\varepsilon_{xx1} = \frac{\partial u_t}{\partial x} + \frac{1}{2} \left( \frac{\partial w_t}{\partial x} \right)^2$$

$$\gamma_{xz} = \frac{\partial u_c}{\partial z} + \frac{\partial w_c}{\partial x}$$

$$\varepsilon_{xx3} = \frac{\partial u_b}{\partial x} + \frac{1}{2} \left( \frac{\partial w_b}{\partial x} \right)^2 \quad (4)$$

式中下标 1 表示上面板, 下标 3 表示下面板.

将式(3)代入(4)式并整理得:

$$\begin{Bmatrix} \boldsymbol{\varepsilon}_{xx1} \\ \boldsymbol{\varepsilon}_{xx3} \\ \boldsymbol{\gamma}_{xz} \end{Bmatrix} = \begin{Bmatrix} \boldsymbol{\varepsilon}_{xx1}^{(0)} \\ \boldsymbol{\varepsilon}_{xx3}^{(0)} \\ \boldsymbol{\gamma}_{xz}^{(0)} \end{Bmatrix} + z \begin{Bmatrix} \boldsymbol{\varepsilon}_{xx1}^{(1)} \\ \boldsymbol{\varepsilon}_{xx3}^{(1)} \\ \boldsymbol{\gamma}_{xz}^{(1)} \end{Bmatrix} \quad (5)$$

其中,

$$\begin{Bmatrix} \boldsymbol{\varepsilon}_{xx1}^{(0)} \\ \boldsymbol{\varepsilon}_{xx3}^{(0)} \\ \boldsymbol{\gamma}_{xz}^{(0)} \end{Bmatrix} = \begin{Bmatrix} \frac{\partial u_0}{\partial x} + \frac{h_c}{2} \left( \frac{\partial \varphi_x}{\partial x} - \frac{\partial^2 w_0}{\partial x^2} \right) + \frac{1}{2} \left( \frac{\partial w_0}{\partial x} \right)^2 \\ \frac{\partial u_0}{\partial x} - \frac{h_c}{2} \left( \frac{\partial \varphi_x}{\partial x} - \frac{\partial^2 w_0}{\partial x^2} \right) + \frac{1}{2} \left( \frac{\partial w_0}{\partial x} \right)^2 \\ -\varphi_x + \frac{\partial w_0}{\partial x} \end{Bmatrix}$$

$$\begin{Bmatrix} \boldsymbol{\varepsilon}_{xx1}^{(1)} \\ \boldsymbol{\varepsilon}_{xx3}^{(1)} \\ \boldsymbol{\gamma}_{xz}^{(1)} \end{Bmatrix} = \begin{Bmatrix} -\frac{\partial^2 w_0}{\partial x^2} \\ \frac{\partial^2 w_0}{\partial x^2} \\ 0 \end{Bmatrix}$$

Hamilton 原理可表述为:

$$\int_{t_1}^{t_2} (\delta U + \delta W - \delta K) dt = 0 \quad (6)$$

式中的  $\delta U$ 、 $\delta W$  和  $\delta K$  分别表示如下:

$$\delta U = \int_{\Omega_0} \left\{ \int_{-h/2}^{h/2} [\sigma_{xx1} (\delta \boldsymbol{\varepsilon}_{xx1}^{(0)} + z \delta \boldsymbol{\varepsilon}_{xx1}^{(1)}) + \sigma_{xx3} (\delta \boldsymbol{\varepsilon}_{xx3}^{(0)} + z \delta \boldsymbol{\varepsilon}_{xx3}^{(1)}) + \sigma_{xz} \delta \boldsymbol{\gamma}_{xz}^{(0)}] dz \right\} dx dy \quad (7a)$$

$$\delta W = - \int_{\Omega_0} [F \cos(\Omega t) \delta w_0 - \mu \dot{w}_0 \delta w_0] dx dy \quad (7b)$$

$$\delta K = \int_{\Omega_0} \int_{-h/2}^{h/2} \rho_1 \left[ (\dot{u}_0 + \frac{h_c}{2} \dot{\varphi}_x - \frac{h_c}{2} \dot{w}_{0,x} - z \dot{w}_{0,x}) \cdot (\delta \dot{u}_0 + \frac{h_c}{2} \delta \dot{\varphi}_x - \frac{h_c}{2} \delta \dot{w}_{0,x} - z \delta \dot{w}_{0,x}) + \dot{w}_0 \delta \dot{w}_0 \right] + \rho_3 \left[ (\dot{u}_0 - \frac{h_c}{2} \dot{\varphi}_x + \frac{h_c}{2} \dot{w}_{0,x} - z \dot{w}_{0,x}) (\delta \dot{u}_0 - \frac{h_c}{2} \delta \dot{\varphi}_x + \frac{h_c}{2} \delta \dot{w}_{0,x} - z \delta \dot{w}_{0,x}) + \dot{w}_0 \delta \dot{w}_0 \right] + \rho_c \left[ (\dot{u}_0 - z \dot{\varphi}_x) (\delta \dot{u}_0 - z \delta \dot{\varphi}_x) + \dot{w}_0 \delta \dot{w}_0 \right] dz dx dy \quad (7c)$$

其中  $\rho_1$ 、 $\rho_3$  分别为上下蒙皮的密度, 由于上下蒙皮与芯层采用相同材料, 故  $\rho_1 = \rho_3 = \rho$ ,  $F \cos(\Omega t)$  为夹芯梁受到的外力,  $\mu$  为阻尼系数. 考虑夹芯梁只发生线弹性变形, 所以满足胡克定律, 有以下应力应变关系:

$$\begin{aligned} \sigma_{xx1} &= E \boldsymbol{\varepsilon}_{xx1} \\ \sigma_{xx3} &= E \boldsymbol{\varepsilon}_{xx3} \\ \sigma_{xz} &= G_c \boldsymbol{\gamma}_{xz} \end{aligned} \quad (8)$$

将式(5)(8)代入(7)式并整理如下:

$$\delta U = \int_{\Omega_0} (N_{xx1} \delta u_{0,x} + \frac{h_c}{2} N_{xx1} \delta \varphi_{x,x} - \frac{h_c}{2} N_{xx1} \delta w_{0,xx} + N_{xx1} w_{0,x} \delta w_{0,x} - M_{xx1} \delta w_{0,xx} + N_{xx3} \delta u_{0,x} - \frac{h_c}{2} N_{xx3} \delta \varphi_{x,x} + \frac{h_c}{2} N_{xx3} \delta w_{0,xx} + N_{xx3} w_{0,x} \delta w_{0,x} - M_{xx3} \delta w_{0,xx} - Q_x \delta \varphi_x + Q_x \delta w_{0,x}) dx dy \quad (9a)$$

$$\delta W = - \int_{\Omega_0} [F \cos(\Omega t) \delta w_0 - \mu \dot{w}_0 \delta w_0] dx dy \quad (9b)$$

$$\delta K = \int_{\Omega_0} [2I_{10} (\dot{u}_0 \delta \dot{u}_0 + \frac{h_c^2}{4} \dot{\varphi}_x \delta \dot{\varphi}_x - \frac{h_c^2}{4} \dot{\varphi}_x \delta \dot{w}_{0,x} - \frac{h_c^2}{4} \dot{w}_{0,x} \delta \dot{\varphi}_x + \frac{h_c^2}{4} \dot{w}_{0,x} \delta \dot{w}_{0,x} + \dot{w}_0 \delta \dot{w}_0) + 2I_{11} (-\frac{h_c}{2} \dot{\varphi}_x \delta \dot{w}_{0,x} + h_c \dot{w}_{0,x} \delta \dot{u}_{0,x} - \frac{h_c}{2} \dot{w}_{0,x} \delta \dot{\varphi}_x) - \frac{h_c^2}{4} \dot{w}_{0,x} \delta \dot{\varphi}_x + \frac{h_c^2}{4} \dot{w}_{0,x} \delta \dot{w}_{0,x} + \dot{w}_0 \delta \dot{w}_0) + I_{21} (-\dot{u}_0 \delta \dot{\varphi}_x - \dot{\varphi}_x \delta \dot{u}_0) + I_{22} \dot{\varphi}_x \delta \dot{\varphi}_x] dx dy \quad (9c)$$

其中,

$$\begin{Bmatrix} N_{xx1} \\ N_{xx3} \end{Bmatrix} = \int_{-h/2}^{h/2} \begin{Bmatrix} \sigma_{xx1} \\ \sigma_{xx3} \end{Bmatrix} dz$$

$$\begin{Bmatrix} M_{xx1} \\ M_{xx3} \end{Bmatrix} = \int_{-h/2}^{h/2} \begin{Bmatrix} \sigma_{xx1} \\ \sigma_{xx3} \end{Bmatrix} z dz$$

$$\begin{Bmatrix} I_{10} \\ I_{11} \\ I_{12} \end{Bmatrix} = \int_{-h/2}^{h/2} \begin{Bmatrix} 1 \\ z \\ z^2 \end{Bmatrix} \rho_1 dz = \int_{h_c/2}^{h/2} \begin{Bmatrix} 1 \\ -z \\ z^2 \end{Bmatrix} \rho_3 dz$$

$$\begin{Bmatrix} I_{20} \\ I_{21} \\ I_{22} \end{Bmatrix} = \int_{-h/2}^{h/2} \begin{Bmatrix} 1 \\ z \\ z^2 \end{Bmatrix} \rho_c dz$$

$$Q_x = \int_{-h/2}^{h/2} \sigma_{xz} dz \quad (10)$$

将式(9)代入方程(6)可得:

$$\int_{t_1}^{t_2} \int_{\Omega_0} \left\{ (N_{xx1} \delta u_{0,x} + \frac{h_c}{2} N_{xx1} \delta \varphi_{x,x} - \frac{h_c}{2} N_{xx1} \delta w_{0,xx} + N_{xx1} w_{0,x} \delta w_{0,x} - M_{xx1} \delta w_{0,xx} + N_{xx3} \delta u_{0,x} - \frac{h_c}{2} N_{xx3} \delta \varphi_{x,x} + \frac{h_c}{2} N_{xx3} \delta w_{0,xx} + N_{xx3} w_{0,x} \delta w_{0,x} - M_{xx3} \delta w_{0,xx} - Q_x \delta \varphi_x + Q_x \delta w_{0,x}) - [F \cos(\Omega t) \delta w_0 - \mu \dot{w}_0 \delta w_0] \right\} dx dy$$

$$\begin{aligned} & \mu \dot{w}_0 \delta w_0 ] - [ 2I_{10} (\dot{u}_0 \delta \dot{u}_0 + \frac{h_c^2}{4} \varphi_x \delta \varphi_x - \frac{h_c^2}{4} \varphi_x \delta \dot{w}_{0,x} - \\ & \frac{h_c^2}{4} \dot{w}_{0,x} \delta \varphi_x + \frac{h_c^2}{4} \dot{w}_{0,x} \delta \dot{w}_{0,x} + \dot{w}_0 \delta \dot{w}_0 ) + \\ & 2I_{11} ( -\frac{h_c}{2} \varphi_x \delta \dot{w}_{0,x} + h_c \dot{w}_{0,x} \delta \dot{w}_{0,x} - \frac{h_c}{2} \dot{w}_{0,x} \delta \varphi_x ) + \\ & 2I_{12} \dot{w}_{0,x} \delta \dot{w}_{0,x} + I_{20} ( \dot{u}_0 \delta \dot{u}_0 + \dot{w}_0 \delta \dot{w}_0 ) + \\ & I_{21} ( -\dot{u}_0 \delta \varphi_x - \varphi_x \delta \dot{u}_0 ) + I_{22} \varphi_x \delta \varphi_x ] \} dx dy dt = 0 \end{aligned} \quad (11)$$

因此,点阵夹芯梁的非线性动力学方程为:

$$(N_{xx1} + N_{xx3})_{,x} = (2I_{10} + I_{20}) \ddot{u}_0 - I_{21} \ddot{\varphi}_x \quad (12a)$$

$$\begin{aligned} & \frac{h_c}{2} (N_{xx1} - N_{xx3})_{,x} + Q_x = (\frac{h_c^2}{2} I_{10} + I_{22}) \ddot{\varphi}_x - \\ & (\frac{h_c^2}{2} I_{10} + h_c I_{11}) \ddot{w}_{0,x} - I_{21} \ddot{u}_0 \end{aligned} \quad (12b)$$

$$\begin{aligned} & (N_{xx1} \frac{\partial w_0}{\partial x} + N_{xx3} \frac{\partial w_0}{\partial x})_{,x} + \frac{h_c}{2} (N_{xx1} - N_{xx3})_{,xx} + \\ & (M_{xx1} + M_{xx3})_{,xx} + Q_{x,x} + F \cos(\Omega t) - \mu \dot{w}_0 = \\ & (\frac{h_c^2}{2} I_{10} + h_c I_{11}) \ddot{\varphi}_{x,x} - (\frac{h_c^2}{2} I_{10} + 2h_c I_{11} + \\ & 2I_{12}) \ddot{w}_{0,xx} + (2I_{10} + I_{20}) \ddot{w}_0 \end{aligned} \quad (12c)$$

方程中的广义力和力矩可由下面的关系表示:

$$\begin{aligned} & N_{xx1} = A_1 \varepsilon_{xx1}^{(0)} + B_1 \varepsilon_{xx1}^{(1)}, N_{xx3} = A_3 \varepsilon_{xx3}^{(0)} + B_3 \varepsilon_{xx3}^{(1)} \\ & M_{xx1} = B_1 \varepsilon_{xx1}^{(0)} + D_1 \varepsilon_{xx1}^{(1)}, M_{xx3} = B_3 \varepsilon_{xx3}^{(0)} + D_3 \varepsilon_{xx3}^{(1)} \\ & Q_x = C \gamma_{xz}^{(0)} \end{aligned} \quad (13)$$

其中,

$$\begin{aligned} & C = \int_{-\frac{h_c}{2}}^{\frac{h_c}{2}} G_c dz \\ & (A_1, B_1, D_1) = \int_{-\frac{h}{2}}^{\frac{h}{2}} E(1, z, z^2) dz \\ & (A_3, B_3, D_3) = \int_{\frac{h}{2}}^{\frac{h}{2}} E(1, z, z^2) dz \end{aligned} \quad (14)$$

从上式可以看出:  $A_1 = A_3, B_1 = -B_3, D_1 = D_3$ .

将式(13)、(14)代入式(12),获得由位移表示的非线性动力学方程:

$$2A_1 u_{0,xx} + 2A_1 w_{0,x} w_{0,xx} = (2I_{10} + I_{20}) \ddot{u}_0 - I_{21} \ddot{\varphi}_x \quad (15a)$$

$$\begin{aligned} & \frac{h_c^2}{2} A_1 \varphi_{x,xx} - \frac{h_c^2}{2} A_1 w_{0,xxx} - h_c B_1 w_{0,xxx} - C \varphi_x + C w_{0,x} \\ & = (\frac{h_c^2}{2} I_{10} + I_{22}) \ddot{\varphi}_x - (\frac{h_c^2}{2} I_{10} + h_c I_{11}) \ddot{w}_{0,x} - I_{21} \ddot{u}_0 \end{aligned} \quad (15b)$$

$$\begin{aligned} & 2A_1 u_{0,xx} w_{0,x} + 2A_1 u_{0,x} w_{0,xx} + 3A_1 w_{0,x}^2 w_{0,xx} + \\ & (\frac{h_c^2}{2} A_1 + h_c B_1) \varphi_{x,xxx} - (\frac{h_c^2}{2} A_1 + 2h_c B_1 + 2D_1) w_{0,xxxx} - \\ & C \varphi_{x,x} + C w_{0,xx} - \mu \dot{w}_0 = (\frac{h_c^2}{2} I_{10} + h_c I_{11}) \ddot{\varphi}_{x,x} - \\ & (\frac{h_c^2}{2} I_{10} + 2h_c I_{11} + 2I_{12}) \ddot{w}_{0,xx} + (2I_{10} + I_{20}) \ddot{w}_0 - \\ & F \cos(\Omega t) \end{aligned} \quad (15c)$$

由于面内惯性和转动惯性相对较小,为了计算方便,忽略其惯性项得:

$$2A_1 u_{0,xx} + 2A_1 w_{0,x} w_{0,xx} = 0 \quad (16a)$$

$$\begin{aligned} & \frac{h_c^2}{2} A_1 \varphi_{x,xx} - \frac{h_c^2}{2} A_1 w_{0,xxx} - h_c B_1 w_{0,xxx} - C \varphi_x + C w_{0,x} = 0 \\ & \end{aligned} \quad (16b)$$

$$\begin{aligned} & 2A_1 u_{0,xx} w_{0,x} + 2A_1 u_{0,x} w_{0,xx} + 3A_1 w_{0,x}^2 w_{0,xx} + \\ & (\frac{h_c^2}{2} A_1 + h_c B_1) \varphi_{x,xxx} - (\frac{h_c^2}{2} A_1 + 2h_c B_1 + 2D_1) w_{0,xxxx} - \\ & C \varphi_{x,x} + C w_{0,xx} - \mu \dot{w}_0 = (2I_{10} + I_{20}) \ddot{w}_0 - F \cos(\Omega t) \end{aligned} \quad (16c)$$

由于夹芯梁两端简支,所以各方向上的解及激励力  $F$  可设为:

$$u_0 = u_1 \sin(\frac{2\pi x}{l}) + u_2 \sin(\frac{4\pi x}{l}) + u_3 \sin(\frac{6\pi x}{l}) \quad (17a)$$

$$w_0 = w_1 \sin(\frac{\pi x}{l}) + w_2 \sin(\frac{2\pi x}{l}) + w_3 \sin(\frac{3\pi x}{l}) \quad (17b)$$

$$\varphi_x = \varphi_1 \cos(\frac{\pi x}{l}) + \varphi_2 \cos(\frac{2\pi x}{l}) + \varphi_3 \cos(\frac{3\pi x}{l}) \quad (17c)$$

$$F = f \sin(\frac{\pi x}{l}) + f \sin(\frac{2\pi x}{l}) + f \sin(\frac{3\pi x}{l}) \quad (17d)$$

将式(17)代入式(16)并运用伽辽金法,获得点阵夹芯梁三自由度的非线性常微分动力学方程:

$$\begin{aligned} & S \frac{\partial^2 w_1}{\partial t^2} + \frac{1}{2} \mu l \frac{\partial w_1}{\partial t} + S_1 w_1 + \left[ \frac{3\pi^4 A_1 w_2^2}{l^3} + \right. \\ & \left. \frac{9 w_3^2 \pi^4 A_1}{4 l^3} \right] w_1 + \frac{1 w_1^3 \pi^4 A_1}{4 l^3} + \frac{3 w_3 w_2^2 \pi^4 A_1}{l^3} \\ & = \frac{l f \cos(\Omega t)}{2} \\ & S \frac{\partial^2 w_2}{\partial t^2} + \frac{1}{2} \mu l \frac{\partial w_2}{\partial t} + S_2 w_2 + \left[ \frac{6\pi^4 A_1 w_3 w_1}{l^3} + \right. \end{aligned} \quad (18a)$$

$$\left. \frac{3\pi^4 A_1 w_1^2 + 27w_3^2 \pi^4 A_1}{l^3} \right] w_2 + \frac{4w_2^3 \pi^4 A_1}{l^3} = \frac{lf \cos(\Omega t)}{2} \quad (18b)$$

$$S \frac{\partial^2 w_3}{\partial t^2} + \frac{1}{2} \mu l \frac{\partial w_3}{\partial t} + S_3 w_3 + \left[ \frac{27\pi^4 A_1 w_2^2}{l^3} + \frac{9w_1^2 \pi^4 A_1}{4l^3} \right] w_3 + \frac{81w_3^3 \pi^4 A_1}{4l^3} + \frac{3w_1 w_2^2 \pi^4 A_1}{l^3} = \frac{lf \cos(\Omega t)}{2} \quad (18c)$$

其中,

$$S = I I_{10} + \frac{1}{2} I I_{20}$$

$$S_1 = \frac{\pi^2 C}{2l} + \frac{\pi^4 A_1 h_c^2 + 4\pi^4 D_1 + 4\pi^4 B_1 h_c}{4l^3} - \frac{\pi^4 C A_1 h_c^2 + 2\pi^4 C B_1 h_c + l^2 \pi^2 C^2}{l(A_1 \pi^2 h_c^2 + 2Cl^2)} - \frac{\pi^6 A_1^2 h_c^4 + 4\pi^6 A_1 h_c^3 B_1 + 4\pi^6 h_c^3 B_1^2}{4l^3(A_1 \pi^2 h_c^2 + 2Cl^2)}$$

$$S_2 = \frac{2\pi^2 C}{l} + \frac{16\pi^4 D_1 + 4\pi^4 A_1 h_c^2 + 16\pi^4 B_1 h_c}{l^3} - \frac{8\pi^4 C A_1 h_c^2 + 16\pi^4 C B_1 h_c + 2l^2 \pi^2 C^2}{l(2A_1 \pi^2 h_c^2 + Cl^2)} - \frac{8\pi^6 A_1^2 h_c^4 + 32\pi^6 A_1 h_c^3 B_1 + 32\pi^6 h_c^3 B_1^2}{l^3(2A_1 \pi^2 h_c^2 + Cl^2)}$$

$$S_3 = \frac{9\pi^2 C}{2l} + \frac{81\pi^4 A_1 h_c^2 + 324\pi^4 D_1 + 324\pi^4 B_1 h_c}{4l^3} - \frac{81\pi^4 C A_1 h_c^2 + 162\pi^4 C B_1 h_c + 9l^2 \pi^2 C^2}{l(9A_1 \pi^2 h_c^2 + 2Cl^2)} - \frac{729\pi^6 A_1^2 h_c^4 + 2916\pi^6 A_1 h_c^3 B_1 + 2916\pi^6 h_c^3 B_1^2}{4l^3(A_1 \pi^2 h_c^2 + 2Cl^2)}$$

## 2 数值验证

本文通过三阶剪切变形理论和有限元仿真两种方法验证所建立方程的正确性。

### 2.1 三阶剪切变形理论

利用三阶剪切变形理论<sup>[16,17]</sup>和哈密顿原理获得点阵夹芯梁转角和横向的动力学方程为:

$$(A_{55} + c_2^2 F_{55} - 2c_2 D_{55}) \left( \frac{\partial^2 w_0}{\partial x^2} + \frac{\partial \varphi_x}{\partial x} \right) - H_{11} c_1^2 \frac{\partial^4 w_0}{\partial x^4} + (c_1 F_{11} - c_1^2 H_{11}) \frac{\partial^3 \varphi_x}{\partial x^3} = I_0 \ddot{w}_0 \quad (19a)$$

$$(D_{11} - 2c_1 F_{11} + c_1^2 H_{11}) \frac{\partial^2 \varphi_x}{\partial x^2} + (-c_1 F_{11} + c_1^2 H_{11}) \frac{\partial^3 w_0}{\partial x^3} + (2c_2 D_{55} - A_{55} - c_2^2 F_{55}) \left( \varphi_x + \frac{\partial w_0}{\partial x} \right) = 0 \quad (19b)$$

其中,

$$c_1 = \frac{4}{3h^2}, \quad c_2 = 3c_1,$$

$$A_{ij} = A_{ij1} + A_{ij3},$$

$$D_{ij} = D_{ij1} + D_{ij3}$$

$$F_{ij} = F_{ij1} + F_{ij3},$$

$$H_{ij} = H_{ij1} + H_{ij3}$$

式中的刚度和惯性矩分别为:

$$(A_{ij1}, B_{ij1}, D_{ij1}, E_{ij1}, F_{ij1}, H_{ij1})$$

$$= \int_{-\frac{h}{2}}^{\frac{h}{2}} E(1, z, z^2, z^3, z^4, z^6) dz$$

$$(A_{ij3}, B_{ij3}, D_{ij3}, E_{ij3}, F_{ij3}, H_{ij3})$$

$$= \int_{\frac{h}{2}}^h E(1, z, z^2, z^3, z^4, z^6) dz \quad (i, j = 1, 2, 6)$$

$$(A_{552}, D_{552}, F_{552}) = \int_{-\frac{h}{2}}^{\frac{h}{2}} G_{xz} (1, z^2, z^4) dz$$

$$I_\alpha = \sum_{k=1}^N \int_{z_k}^{z_{k+1}} \rho^{(k)}(z) z^\alpha dz \quad (\alpha = 0, 1, 2, \dots, 6) \quad (20)$$

### 2.2 有限元仿真

运用UG软件对点阵夹芯梁进行实体建模,模型如图4所示.然后将模型导入ANSYS workbench中进行有限元仿真,采用四面体网格划分,使用patch conforming算法,网格划分如图5所示,梁的两个端面采用简支边界条件.

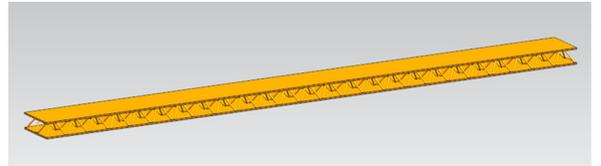


图4 金字塔型点阵夹芯梁模型图

Fig. 4 Model of pyramidal truss core sandwich beam

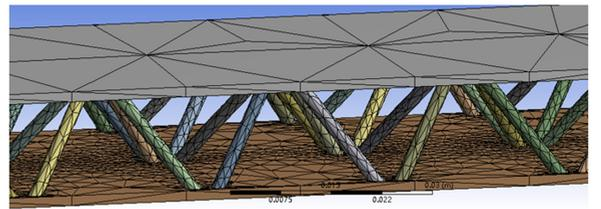


图5 金字塔型点阵夹芯梁的网格划分

Fig. 5 Finite element mesh of pyramidal truss core sandwich beam

### 2.3 固有频率比较

夹芯梁蒙皮和芯层的材料均采用铝合金,材料参数及夹芯梁的结构参数为:材料密度  $\rho = 2770 \text{ kg/m}^3$ , 弹性模量  $E = 71 \text{ GPa}$ , 泊松比  $\nu = 0.33$ , 芯层杆件半径  $r_c = 1 \text{ mm}$ , 杆件倾斜角  $\alpha = 45^\circ$ , 芯层高度  $h_c = 14.14 \text{ mm}$ , 蒙皮厚度  $h_f = 1.5 \text{ mm}$ , 夹芯梁长度方向取 25 个单胞, 宽度方向取 2 个单胞, 单胞的底面边长取  $28 \text{ mm}$ .

表 1 给出的金字塔型点阵夹芯梁前三阶固有频率分别由折线理论、有限元仿真和三阶剪切变形理论得到. 如表 1 所示, 由折线理论计算的点阵夹芯梁固有频率的理论值与仿真结果以及三阶剪切变形理论值在较低阶频率处吻合较好, 阶次越高, 结果的差异越大. 利用三阶剪切变形理论计算的夹芯结构固有频率通常会比实际值大<sup>[18,19]</sup>.

表 1 金字塔型点阵夹芯梁的固有频率

Table 1 Natural frequencies of pyramidal truss core sandwich beam

	the first-order	the second-order	the third-order
Present (Hz)	116.55	423.86	840.30
Simulation (Hz)	114.93	403.04	766.88
TSDT (Hz)	118.64	450.85	940.91

### 3 结构参数对夹芯梁固有频率的影响

为了得到无量纲的动力学方程, 引入下式:

$$\begin{aligned} \bar{u}_0 &= \frac{u_0}{l}, \quad \bar{w}_0 = \frac{w_0}{h}, \quad \bar{\varphi}_x = \frac{\varphi_x}{l}, \quad \bar{x} = \frac{x}{l}, \quad \bar{F} = \frac{l^4}{Eh^4}F, \\ \bar{\mu} &= \frac{l^2}{h^2} \left( \frac{1}{\rho E} \right)^{1/2} \mu, \quad \bar{t} = \frac{h}{l^2} \left( \frac{E}{\rho} \right)^{1/2} t, \quad \bar{h}_c = \frac{h_c}{h}, \\ \bar{\Omega} &= \frac{l^2}{h} \left( \frac{\rho}{E} \right)^{1/2} \Omega, \quad \bar{A}_i = \frac{l}{Eh^2} A_i, \quad \bar{B}_i = \frac{l}{Eh^3} B_i, \\ \bar{C} &= \frac{l}{Eh^2} C, \quad \bar{D}_i = \frac{l}{Eh^4} D_i, \quad \bar{I}_{ii} = \frac{1}{l^{(i+1)} \rho} I_{ii} \end{aligned} \quad (21)$$

式(16)无量纲化后可以写成下式, 为了表述方便, 忽略无量纲量上的“-”有,

$$\frac{2h^2 A_1 u_{0,xx}}{l^2} + \frac{2h^4 A_1 w_{0,x} w_{0,xx}}{l^4} = 0 \quad (22a)$$

$$\begin{aligned} \frac{h^3 h_c^2 A_1 \varphi_{x,xx}}{2l^3} - \frac{h^4 h_c^2 A_1 w_{0,xxx}}{2l^4} - \frac{h^4 h_c B_1 w_{0,xxx}}{l^4} - \\ \frac{hC\varphi_x}{l} + \frac{h^2 C w_{0,x}}{l^2} = 0 \end{aligned} \quad (22b)$$

$$\begin{aligned} 2A_1 u_{0,xx} w_{0,x} + 2A_1 u_{0,x} w_{0,xx} + \frac{3h^2 A_1 w_{0,x}^2 w_{0,xx}}{l^2} + \\ \left( \frac{h_c^2 A_1}{2} + h_c B_1 \right) \frac{h\varphi_{x,xxx}}{l} - \left( \frac{h_c^2}{2} A_1 + 2h_c B_1 + \right. \\ \left. 2D_1 \right) \frac{h^2 w_{0,xxxx}}{l^2} - \frac{lC\varphi_{x,x}}{h} + C w_{0,xx} - \frac{h\mu w_{0,t}}{l} \\ = (2I_{10} + I_{20}) w_{0,t} - \frac{hF}{l} \cos(\Omega t) \end{aligned} \quad (22c)$$

下面主要研究点阵夹芯梁杆件半径、杆件倾斜角度以及芯层高度的变化对点阵夹芯梁无量纲化固有频率的影响. 具体方法是仅改变夹芯梁的一个结构参数并保持其他的结构参数不变, 计算夹芯梁的固有频率. 结果如表 2~4 所示.

表 2 不同杆半径下金字塔型点阵夹芯梁固有频率

( $r_c = 0.4 \sim 1.9 \text{ mm}$ ,  $\alpha = 45^\circ$ ,  $L = 800 \text{ mm}$ ,  $h_c = 15 \text{ mm}$ ,  $h = 18 \text{ mm}$ )

Table 2 Natural frequencies of pyramidal truss core sandwich beam with different truss radii

( $r_c = 0.4 \sim 1.9 \text{ mm}$ ,  $\alpha = 45^\circ$ ,  $L = 800 \text{ mm}$ ,  $h_c = 15 \text{ mm}$ ,  $h = 18 \text{ mm}$ )

$r_c/h$	the first-order	the second-order	the third-order
0.0222	4.00625	12.7309	22.5635
0.0389	4.18210	15.0456	29.4914
0.0556	4.12553	15.5292	32.0241
0.0723	4.00749	15.4003	32.6259
0.0890	3.86910	15.0386	32.3626
0.1057	3.72827	14.5890	31.7068

表 3 不同杆件倾斜角度下金字塔型点阵夹芯梁固有频率

( $r_c = 1.0 \text{ mm}$ ,  $\alpha = 30^\circ \sim 60^\circ$ ,  $L = 800 \text{ mm}$ ,  $h_c = 15 \text{ mm}$ )

Table 3 Natural frequencies of pyramidal truss core sandwich beam with different inclination angles

( $r_c = 1.0 \text{ mm}$ ,  $\alpha = 30^\circ \sim 60^\circ$ ,  $L = 800 \text{ mm}$ ,  $h_c = 15 \text{ mm}$ )

$\alpha$	the first-order	the second-order	the third-order
$30^\circ$	4.12311	14.3269	27.1656
$35^\circ$	4.16053	15.0283	29.5782
$40^\circ$	4.15692	15.3961	31.1376
$45^\circ$	4.12553	15.5292	32.0241
$50^\circ$	4.06694	15.4784	32.3620
$55^\circ$	3.98121	15.2591	32.2123
$60^\circ$	3.85746	14.8580	31.5685

由表 2 可以看出, 随着杆件半径  $r_c$  由  $0.4 \text{ mm}$  增加到  $1.9 \text{ mm}$ , 点阵夹芯梁的固有频率呈先增后减的趋势, 且各阶固有频率达到极值所对应的杆件半径随着阶数的增加而增大. 而且, 各阶固有频率在达到其极值前的变化率比达到极值后的变化率大. 因此有, 随着杆件半径的增加, 点阵夹芯梁的刚度

和等效密度同时增大(刚度增大对夹芯梁的固有频率有增大的作用,而等效密度的增大对夹芯梁的固有频率有减小的作用),在这个过程中夹芯梁的刚度与等效密度共同作用,使得点阵夹芯梁的固有频率先快速的增大后较缓慢的降低。

由表3可以看出,杆件倾斜角度对点阵夹芯梁固有频率的影响与杆件半径对点阵夹芯梁固有频率影响的情况相似,随着杆件倾斜角度的增加,点阵夹芯梁的固有频率先增大后减小,且各阶固有频率在达到极值前的变化率比达到极值后的变化率稍大。同样有,随着杆件倾斜角度的增加,点阵夹芯梁的刚度和等效密度同时增大,在这个过程中夹芯梁的刚度与等效密度共同作用,使得点阵夹芯梁的固有频率呈现先快速增大后较缓慢降低的变化规律。从表2、表3可以看出杆件倾斜角度对金字塔型点阵夹芯梁固有频率的影响相对于杆件半径的影响小。杆件半径、杆件倾斜角度由小到大,点阵夹芯梁高阶的固有频率比低阶的固有频率变化幅度大。

表4 不同芯层高度下金字塔型点阵夹芯梁固有频率

$$(r_c = 1.0\text{mm}, \alpha = 45^\circ, L = 800\text{mm}, h_c = 6 \sim 24\text{mm}, \\ h_f = 1.5\text{mm}, h = h_c + 2h_f)$$

Table 4 Natural frequencies of pyramidal truss core sandwich beam with different core heights

$$(r_c = 1.0\text{mm}, \alpha = 45^\circ, L = 800\text{mm}, h_c = 6 \sim 24\text{mm}, \\ h_f = 1.5\text{mm}, h = h_c + 2h_f)$$

$h_c/h$	the first-order	the second-order	the third-order
2/3	3.65509	14.5350	32.3908
3/4	3.89872	15.3460	33.6360
4/5	4.04599	15.6339	33.3733
5/6	4.12553	15.5292	32.0241
6/7	4.15572	15.1208	29.9845
7/8	4.14608	14.4893	27.6100
8/9	4.10366	13.7113	25.1690

从表4可以看出,芯子高度对点阵夹芯梁固有频率的影响与杆件半径、杆件倾斜角度对点阵夹芯梁固有频率影响的情况相似。随着芯子高度的增加,点阵夹芯梁的固有频率先增大后减小,而与前者不同的是,点阵夹芯梁各阶固有频率达到极值所对应的芯子高度随着阶数的增加而减小。因此,在芯子变化的过程中夹芯梁上下蒙皮的厚度不变,随着芯层高度的增加,上下蒙皮的距离不断增加,夹芯梁的截面惯性矩也随之快速增大,这对于横向振动梁固有频率的影响是相当大的。随着芯层高度的增加,杆件半径不变,芯子的等效密度逐渐减小,

芯子的剪切刚度同样逐渐减小,使得梁的固有频率呈减小的趋势。

由表2到表4可以看出,杆件半径、杆件倾斜角度或芯子高度的改变都会引起刚度和惯性的变化。无论哪个结构参数,对固有频率的影响都是相当复杂的。因此点阵夹芯结构在实际应用中,必须对材料和结构参数经过合理的优化。

#### 4 点阵夹芯梁在不同激振力下的非线性响应

取  $r_c = 1.0\text{mm}$ ,  $\alpha = 45^\circ$ ,  $L = 800\text{mm}$ ,  $h_c = 15\text{mm}$ , 获得点阵夹芯梁的振动方程为:

$$\frac{\partial^2 w_1}{\partial t^2} + 5.2\mu \frac{\partial w_1}{\partial t} + 17.018w_1 + 21.107w_1^3 + \\ 253.279w_2^2w_1 + 189.960w_3^2w_1 + 253.279w_3w_2^2 \\ = 5.2f\cos(\Omega t) \quad (23a)$$

$$\frac{\partial^2 w_2}{\partial t^2} + 5.2\mu \frac{\partial w_2}{\partial t} + 241.157w_2 + 337.706w_2^3 + \\ 253.279w_1^2w_2 + 506.559w_3w_1w_2 + \\ 2279.515w_3^2w_2 = 5.2f\cos(\Omega t) \quad (23b)$$

$$\frac{\partial^2 w_3}{\partial t^2} + 5.2\mu \frac{\partial w_3}{\partial t} + 1025.587w_3 + 1709.636w_3^3 + \\ 253.279w_1w_2^2 + 189.960w_3w_1^2 + 2279.515w_3w_2^2 \\ = 5.2f\cos(\Omega t) \quad (23c)$$

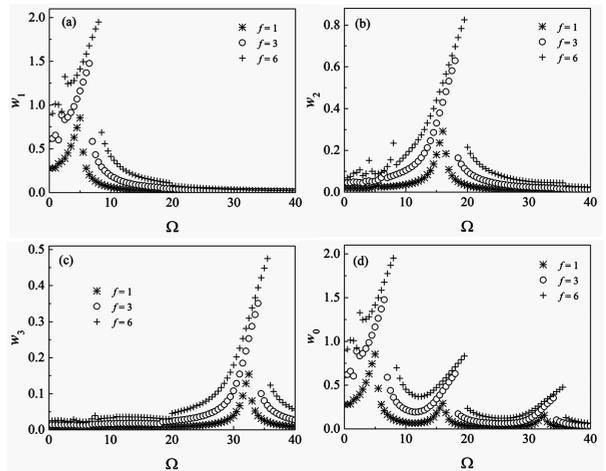


图6 金字塔型点阵夹芯梁在不同大小激振力下的幅频响应 (a)第一阶模态 (b)第二阶模态 (c)第三阶模态 (d)总响应  
Fig. 6 Frequency responses of pyramid truss core sandwich beam under different excitation amplitudes (a) the first mode (b) the second mode (c) the third mode (d) total responses

运用 Matlab 程序对方程(23)进行数值仿真,取  $\mu = 0.2$ ,  $f = 1, 3, 6$ 。利用龙格库塔法获得点阵夹芯梁在不同激振力下的非线性响应,如图6所示。本节主要关注激励参数和结构参数对点阵夹芯梁硬

特性非线性、超谐共振响应的影响,故采用该方法进行研究.关于其他非线性特征,若采用此方法进行研究则存在一定局限.

如图6d所示,当 $f=1$ 时,金字塔型点阵夹芯梁的频响曲线表现出较弱的非线性,在各阶固有频率处出现较低的共振峰,且随着阶数的增加,峰值逐渐减小.金字塔型点阵夹芯梁的振幅随着激励的增大而增大.随着激励的增大,图中各阶模态幅频响应曲线的共振峰值全部右移,夹芯梁各阶模态的硬特性变得更加明显.并且,各阶模态达到共振峰值后发生的振幅跳跃现象也越明显,各阶模态共振频带逐渐变宽.由图可以看出,第一阶模态的非线性响应随激励幅值的变化最为明显.当 $f=3$ 时,第一阶和第二阶模态的幅频响应曲线,如图6a、b所示,在低频激励段出现较小的突起,点阵夹芯梁出现了超谐共振,即较低频率的激励引起较高频率的响应.当 $f=6$ 时,第一阶和第二阶模态的超谐共振峰值增大,并且可以看出跳跃现象更加明显且共振频带进一步变宽.

### 5 不同芯层参数下点阵夹芯梁的非线性响应

本节研究金字塔型点阵夹芯梁杆件半径、杆件倾斜角度和芯子高度对非线性幅频响应的影响.具体方法是在相同的激励幅值下改变其中的一个结构参数,并保持其他的参数不变,获得幅频响应曲线并进行分析.其中 $\mu=0.2, f=6$ ,幅频响应曲线如图7~9所示.

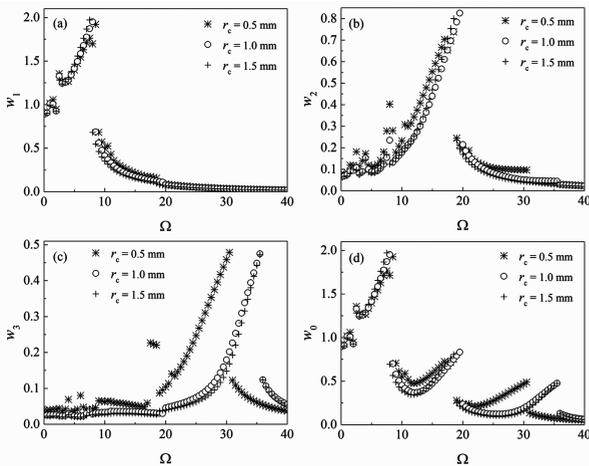


图7 不同的杆件半径下的幅值响应曲线

(a) 第一阶模态 (b) 第二阶模态 (c) 第三阶模态 (d) 总响应  
Fig. 7 Frequency response of pyramid truss core sandwich beam with different strut radii (a) the first mode (b) the second mode (c) the third mode (d) total responses

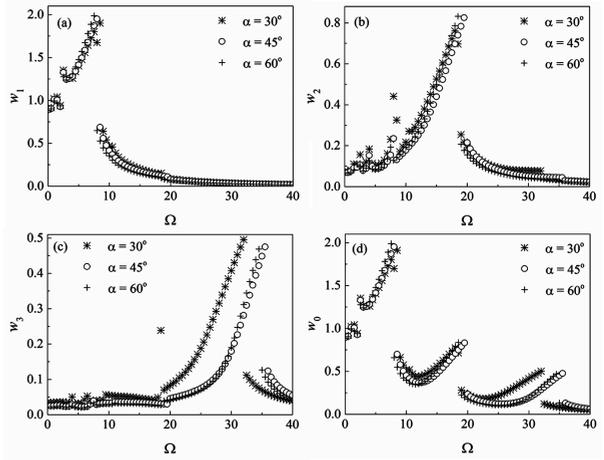


图8 不同的杆件倾斜角度下的幅值响应曲线

(a) 第一阶模态 (b) 第二阶模态 (c) 第三阶模态 (d) 总响应  
Fig. 8 Frequency response of pyramid truss core sandwich beam with different inclination angles (a) the first mode (b) the second mode (c) the third mode (d) total responses

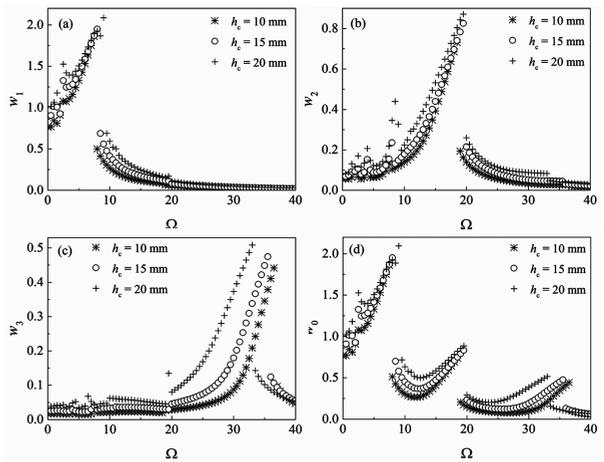


图9 不同的芯层高度下的幅值响应曲线

(a) 第一阶模态 (b) 第二阶模态 (c) 第三阶模态 (d) 总响应  
Fig. 9 Frequency response of pyramid lattice truss core sandwich beam with different core heights (a) the first mode (b) the second mode (c) the third mode (d) total responses

如图7所示,当杆件半径分别为0.5mm、1.0mm、1.5mm时,第一阶模态共振峰的形状变化较小,即幅频响应曲线所表现出的硬特性非线性、共振峰处的跳跃和频带宽度发生的变化相对较小.由于具有不同杆件半径的点阵夹芯梁的第三阶固有频率存在较大差异,故其第三阶模态的幅频响应与其他两阶模态存在较明显的变化.如图7a所示,当杆件半径变化时,第一阶模态处发生的超谐共振幅值基本保持不变.图7b表示,当杆件半径逐渐减小时,第二阶模态的超谐共振逐渐增强,该模态主共振的最大振幅在 $r_c=0.5\text{mm}$ 时最小,在 $r_c=1.0\text{mm}$

时最大.如图7c所示,当杆件半径最小,即 $r_c = 0.5$  mm时,激励力处于较低频段即可引起第三阶模态的响应,尤其是激励频率处于18附近时,产生了较大幅度的响应.

如图8所示,当杆件倾斜角度分别为 $30^\circ$ 、 $45^\circ$ 、 $60^\circ$ 时,各阶模态幅频响应曲线均显示出硬特性非线性.当杆件倾斜角度变化时,第一阶模态的响应峰值基本保持不变,如图8a所示.图8b中,当杆件倾斜角度逐渐减小时,第二阶模态处的超谐共振幅值逐渐增大.与杆件半径的影响相同,杆件倾斜角度的变化也引起了共振峰值所对应的频率的变化.图9为芯层厚度分别取10mm、15mm、20mm时,各阶模态的幅频响应曲线.随着芯层高度的增大,各阶模态的主共振峰值明显增大,尤其是前两阶模态更为显著.各阶模态共振频带逐渐变宽,以第三阶模态最为明显.第一阶模态与第二阶模态的超谐共振幅值同样变大.当芯层高度最大,即 $h_c = 20$  mm时,低频激励对于第三阶模态的影响最大,如图9c所示.

## 6 结论

本文主要研究了结构参数对金字塔型点阵夹芯梁振动特性的影响,有如下结论:

(1)金字塔型点阵夹芯梁的固有频率随着杆件半径的增大呈先增后减的趋势,且各阶固有频率达到极值所对应的杆件半径随着阶数的增加而增大;杆件倾斜角度对点阵夹芯梁固有频率的影响与杆件半径对夹芯梁固有频率影响的规律相同,且杆件倾斜角度对夹芯梁固有频率的影响比较小;芯子高度对点阵夹芯梁固有频率的影响与前两者相似,不同点为各阶固有频率达到极值所对应的芯子高度随着阶数的增加而减小.

(2)金字塔型点阵夹芯梁的幅频响应随着激励幅值的增大而增大.随着激励幅值的增大,各阶模态共振峰值处的跳跃现象更加明显,共振频带逐渐变宽.第一、二阶模态可以发生超谐共振,其响应幅值逐渐增大.芯层结构参数的变化对金字塔型点阵夹芯梁的非线性幅频响应存在较大影响.主共振响应的共振频率、响应振幅和共振频带宽度均会随着芯层结构参数的变化而改变.值得注意的是,相同激励下,通过改变点阵夹芯梁的任一芯层参数,都能够使夹芯梁发生超谐共振,换言之,通过改变

芯层参数,能够避免夹芯梁超谐共振的发生.

## 参 考 文 献

- 1 方岱宁,张一慧,崔晓东. 轻质点阵材料力学与多功能设计. 北京: 科学出版社, 2009 (Fang D N, Zhang Y H, Cui X D. Light lattice truss mechanics of materials and multifunctional design. Beijing: Science Press, 2009 (in Chinese))
- 2 曾嵩,朱荣,姜炜等. 金属点阵材料的研究进展. 材料导报 A: 综述篇, 2012, 26(3): 18~23 (Zeng S, Zhu R, Jiang W, et al. Research progress of metal lattice truss materials. *Materials Review A: Summarization*, 2012, 26(3): 18~23 (in Chinese))
- 3 卢天健,何德坪,陈常青等. 超轻多孔金属材料的多功能特性及应用. 力学进展, 2006, 36(4): 517~535 (Lu T J, He D P, Chen C Q, et al. The multifunctional characteristics of ultra-light porous metal materials and its application. *Advances in Mechanics*, 2006, 36(4): 517~535 (in Chinese))
- 4 杜善义. 先进复合材料与航空航天. 复合材料学报, 2007, 24(1): 1~12 (Du S Y. Advanced composite materials and aerospace. *Acta Materiae Compositae Sinica*, 2007, 24(1): 1~12 (in Chinese))
- 5 Song Z G, Li F M. Aeroelastic analysis and active flutter control of nonlinear lattice sandwich beams. *Nonlinear Dynamics*, 2014, 76(1): 57~68
- 6 娄佳,马力,吴林志. 复合材料四面体点阵夹芯梁的自由振动分析. 固体力学学报, 2011, 32(4): 339~345 (Lou J, Ma L, Wu L Z. Free vibration analysis of composite sandwich beam with tetrahedral lattice truss core. *Acta Mechanica Solida Sinica*, 2011, 32(4): 339~345 (in Chinese))
- 7 Chen J E, Zhang W, Liu J, et al. Dynamic properties of truss core sandwich plate with tetrahedral core. *Composite Structures*, 2015, 134: 869~882
- 8 李拓,江俊. 点阵多孔金属夹芯板振动特性分析及优化设计. 动力学与控制学报, 2009, 7(1): 39~44 (Li T, Jiang J. Vibration analysis and optimization design of porous metal sandwich panels with lattice truss core. *Journal of Dynamics and Control*, 2009, 7(1): 39~44 (in Chinese))
- 9 Kant T, Swaminathan K. Analytical solutions for free vibration of laminated composite and sandwich plates based on a higher-order refined theory. *Composite Structures*, 2001, 53(1): 73~85

- 10 Alijani F, Amabili M. Nonlinear vibrations of laminated and sandwich rectangular plates with free edges. Part 1: Theory and numerical simulations. *Composite Structures*, 2013, 105: 422~436
- 11 Alijani F, Amabili M, Ferrari G, et al. Nonlinear vibrations of laminated and sandwich rectangular plates with free edges. Part 2: Experiments & comparisons. *Composite Structures*, 2013, 105: 437~445
- 12 Won S G, Bae S H, Cho J R, et al. Three-layered damped beam element for forced vibration analysis of symmetric sandwich structures with a viscoelastic core. *Finite Elements in Analysis and Design*, 2013, 68: 39~51
- 13 Allen H G. Analysis and design of structural sandwich panels. Oxford: Pergamon Press, 1969
- 14 Deshpande V S, Fleck N A. Collapse of truss core sandwich beams in 3-point bending. *International Journal of Solids and Structures*, 2001, 38(36-37): 6275~6305
- 15 Simsek M. Fundamental frequency analysis of functionally graded beams by using different higher-order beam theories. *Nuclear Engineering and Design*, 2010, 240: 697~705
- 16 Reddy J N. Mechanics of laminated composite plates and shells: theory and analysis, second edition. Florida: CRC Press, 2003: 671~677
- 17 陈丽华, 孙玥, 张伟. 三阶剪切变形板的振动特性研究. *动力学与控制学报*, 2014, 12(1): 50~55 (Chen L H, Sun Y, Zhang W. Study on vibration characteristic of third order shear deformation theory of plate. *Journal of Dynamics and Control*, 2014, 12(1): 50~55 (in Chinese))
- 18 Ferreira A J M. Analysis of composite plates using a layerwise theory and multiquadrics discretization. *Mechanics of Advanced Materials and Structures*, 2005, 12: 99~112
- 19 Chen J E, Zhang W, Sun M, et al. Parametric study on nonlinear vibration of composite truss core sandwich plate with internal resonance. *Journal of Mechanical Science and Technology*, 2016, 30(9): 4133~4142

## VIBRATION CHARACTERISTICS OF SANDWICH BEAM WITH PYRAMIDAL TRUSS CORE\*

Shi Yueqi   Chen Jianen<sup>†</sup>   Ge Weimin   Liu Jun   Wang Xiaofeng

(Tianjin University of Technology, Tianjin Key Laboratory of the Design and Intelligent Control of  
the Advanced Mechatronical System, Tianjin 300384, China)

**Abstract** The free vibration and nonlinear forced vibration of the sandwich beam with pyramidal truss core were investigated. The zig-zag theory was used to derive the nonlinear dynamic equation for the truss core sandwich beam. The natural frequencies of the sandwich beam were also calculated and verified. The effects of strut radius, inclination angle and core height on the natural frequencies of the sandwich beam were then analyzed. Meanwhile, the nonlinear frequency responses of the sandwich beam under different excitation amplitudes and with different structural parameters were studied. The results show that the natural frequencies of the sandwich beam increased and then decreased with the increase of three structural parameters. In addition, the structural parameters of the truss core exhibited complicated effects on nonlinear responses of the sandwich beam.

**Key words** vibration analysis, truss core sandwich beam, nonlinear frequency response, structural parameter, natural frequency

Received 20 July 2006, revised 9 September 2006.

\* The project supported by the National Natural Science Foundation of China (11402170), Tianjin Natural Science Foundation of China (14JCYBJC19400)

<sup>†</sup> Corresponding author E-mail: vchenje@163.com